

Absorptive potentials due to ionization and thermal diffuse scattering by fast electrons in crystals

L. J. Allen

School of Science and Mathematics Education, University of Melbourne, Parkville, Victoria 3052, Australia

C. J. Rossouw

CSIRO Division of Materials Science and Technology, Normanby Road, Locked Bag 33, Clayton, Victoria 3168, Australia

(Received 5 June 1990)

An expression for the Fourier coefficients of the absorptive potential due to electron-impact ionization in crystals is derived and the cross section is given in terms of these Fourier components. Absorptive potentials due to K -shell ionization and thermal diffuse scattering (TDS) are calculated with use of a hydrogenic model and an Einstein model, respectively. Inelastic potentials require integration over all states of the scattered electron and, for K -shell ionization, integration over all states of the ejected electron. These potentials are thus dependent on incident-beam energy, in contrast with the elastic potential. The projected spatial distribution of these potentials are plotted and compared with the elastic potential for CdTe, GaAs, Si, and diamond. The delocalization of the ionization absorptive potential is similar to that expected from classical impact-parameter arguments. The form of the TDS potential is substantially different from that due to elastic scattering, being extremely peaked on atomic positions with no absorption in the channels between atomic planes.

I. INTRODUCTION

An expression for the potential for atomic ionization in a crystalline environment is derived for the first time in this paper. This leads to an expression for the ionization cross section σ in terms of V_{g-h}'' , the Fourier coefficients of the interaction potential. This formula is of fundamental importance for ionization probabilities measured under strong diffraction conditions by electron-energy-loss spectroscopy (EELS) or energy dispersive x-ray spectroscopy (EDX). The form of this absorptive potential is calculated as a function of incident energy E_0 for atoms from different rows in the Periodic Table, using a modified hydrogenic model for K -shell excitation.¹⁻⁴ The widths and absolute magnitudes of projected potentials for K -shell ionization, $V''(r)$, are compared with the absorptive potential $V'(r)$ due to thermal diffuse scattering (TDS) for different values of E_0 and temperature T , using CdTe, GaAs, silicon, and diamond. In this way we also investigate materials with widely differing Debye temperatures Θ_D and atomic numbers Z .

Anomalous absorption effects due to TDS have been addressed by Whelan,⁵ Hall and Hirsch,⁶ Humphreys and Hirsch,⁷ Doyle⁸ and Radi,⁹ and, more recently, by Rossouw and Bursill.^{10,11} It has been shown¹² that the ratio of the Fourier coefficients of the absorption potential due to TDS on an Einstein model and that for elastic scattering, V'_g/V_g , does not remain constant as the reciprocal-lattice vectors g increase and, for large g , this ratio becomes negative. The physical meaning of this sign inversion is made clear by plotting $V'(r)$ for a number of semiconductor crystals. Implications of phase differences that occur between V'_g and V_g have been discussed by Bird, James, and King.¹³ Wang¹⁴ has developed the theory of TDS using a phonon model¹⁵ and applied it via a multislice diffraction model to phenomena observed in scanning transmission electron microscope (STEM) imaging.¹⁶

However, despite the complex behavior of V'_g/V_g being widely known, a common assumption for inclusion of anomalous absorption in diffraction simulations has been to scale V'_g to V_g via a constant factor, i.e.,

$$V'_g = \alpha V_g, \quad (1)$$

where α commonly lies between 0.02 and 0.1 for a reasonable fit between experiment and theory for all g .^{17,18} Semiconductor quantum-well structures have been investigated by fitting individual atomic absorptive potentials to their elastic counterparts, and deriving composition from optimized correlation between theoretical and experimental thickness fringes.¹⁷⁻¹⁹ In this paper, by explicitly plotting $V'(r)$ for a number of incident beam energies E_0 and for temperatures T of 300 K and absolute zero (to show the effect of zero point energy), we demonstrate why scaling of the absorptive potential to the elastic potential is inappropriate.

II. THEORY

The dynamical equations of Bethe²⁰ are a starting point for a general theory of electron diffraction in a crystal:

$$[K^2 - (\mathbf{k}^i + \mathbf{g})^2]C_g^i + \sum_{h(\neq g)} U_{g-h} C_h^i = 0, \quad (2)$$

there being one equation for each Bloch wave on branch i of the dispersion surface. $K^2 = k^2 + U_0$, where \mathbf{k} is the vacuum wave vector of the fast electron and U_0 is related to the mean inner crystal potential. Inelastic scattering is treated by an absorptive potential, by including an imaginary component in the Fourier coefficient

$$U_{g-h} = \frac{2m}{h^2} V_{g-h}, \quad (3)$$

where m is the relativistic electron mass. The spatial distribution of the total crystal potential is reconstructed

$$f''_{\beta}(\mathbf{g}-\mathbf{h}) = \frac{n}{\pi a_0^{*2}} \int_0^{\kappa_{\max}} k' \kappa^2 \int \frac{1}{Q_g^2 Q_h^2} \left[\int F(\mathbf{Q}_g, \boldsymbol{\kappa}) F^*(\mathbf{Q}_h, \boldsymbol{\kappa}) d\Omega_{\boldsymbol{\kappa}} \right] d\Omega d\kappa, \quad (13)$$

where the factor n is inserted to account for the number of electrons in the initial target shell. We assume K -shell ionization for our calculations ($n=2$) and for which a modified hydrogenic model^{3,4} is adequate in evaluating the transition matrix elements given by Eq. (12). The quantities \mathbf{Q}_g and \mathbf{Q}_h are $\mathbf{q}+\mathbf{g}$ and $\mathbf{q}+\mathbf{h}$, respectively.

An expression for the $(e, 2e)$ differential cross section in a crystal that accounts for dynamical diffraction of both incident electron \mathbf{k} and outgoing electrons \mathbf{k}' and $\boldsymbol{\kappa}$ has recently been published.²⁷ For the case of inner-shell ionization with diffraction included for the incident electron alone, these equations reduce to the following expression consistent with that obtained previously by other authors.^{28,29}

$$\frac{d^3\sigma}{d\Omega d\Omega_{\boldsymbol{\kappa}} dE} = \frac{4n}{(2\pi)^3} \frac{Nm}{a_0^{*2} \hbar^2} \frac{k'\kappa}{k} \mathcal{A}[\text{site}] \mathcal{A}[\text{BW}] \frac{F(\mathbf{Q}_g, \boldsymbol{\kappa}) F^*(\mathbf{Q}_h, \boldsymbol{\kappa})}{Q_g^2 Q_h^2}, \quad (14)$$

$$\mathcal{A}[\text{kin}] = \int k' \kappa^2 \left[\int \frac{1}{Q_g^2 Q_h^2} \left[\int F(\mathbf{Q}_g, \boldsymbol{\kappa}) F^*(\mathbf{Q}_h, \boldsymbol{\kappa}) d\Omega_{\boldsymbol{\kappa}} \right] d\Omega \right] d\kappa. \quad (17)$$

Analytic expressions²⁸⁻³⁰ have been given for the quantity

$$\int F(\mathbf{Q}_g, \boldsymbol{\kappa}') F^*(\mathbf{Q}_h, \boldsymbol{\kappa}) d\Omega_{\boldsymbol{\kappa}}, \quad (18)$$

where, if $\mathbf{Q}_g \neq \mathbf{Q}_h$, these “nondiagonal” terms contribute the site sensitivity and orientation dependence of the ionization cross section. The integration over all final states of both ejected and scattered electrons is illustrated schematically in Fig. 1. For a particular ejected electron wave vector $\boldsymbol{\kappa}$ and for each element \mathbf{Q}_g , \mathbf{Q}_h , and $d\Omega$, integration of $\Omega_{\boldsymbol{\kappa}}$ over all ejection directions is evaluated from Eq. (18). The second integral in Eq. (17) is numerically integrated over 4π steradians for the scattered electron \mathbf{k}' . The first integral is then evaluated with $\boldsymbol{\kappa}$ being incremented by $\Delta\boldsymbol{\kappa}$, and numerical integration over Ω and $\Omega_{\boldsymbol{\kappa}}$ repeated. Comparison of Eqs. (16) and (17) with Eqs. (5) and (13) shows that σ can be expressed as follows:

$$\sigma = \frac{NV_c}{2\pi k} \mathcal{A}[\text{BW}] U''_{h-g}, \quad (19)$$

where the Fourier coefficients

where N is the number of unit cells in the crystal. The term $\mathcal{A}[\text{BW}]$ relates to the Bloch-wave eigenvectors \mathbf{C} and eigenvalues γ of the fast electron wave function in the crystal, and is given by

$$\mathcal{A}[\text{BW}] = \sum_{ij} A^i A^{j*} \frac{\exp\{i(\gamma^i - \gamma^j)d\} - 1}{i(\gamma^i - \gamma^j)d} \sum_{g,h} C_g^i C_h^{j*}, \quad (15)$$

where d is the crystal thickness. Integrating over the appropriate variables in Eq. (14) we obtain the following expression for the total ionization cross section:

$$\sigma = \frac{4n}{(2\pi)^3} \frac{N}{a_0^{*2} k} \mathcal{A}[\text{BW}] \mathcal{A}[\text{site}] \mathcal{A}[\text{kin}], \quad (16)$$

where $\mathcal{A}[\text{BW}]$ and $\mathcal{A}[\text{site}]$ are given by Eqs. (15) and (6), respectively, and the interaction kinematics term

$$U''_{h-g} = \frac{4n}{(2\pi)^2 a_0^{*2} V_c} \mathcal{A}[\text{site}] \mathcal{A}[\text{kin}] \quad (20)$$

so that σ is given in terms of the Fourier coefficients of the ionization potential.

We have assumed a final state of the ejected electron that does not explicitly contain solid-state effects. Integrating over all ejection energies, such effects, responsible, for example, for extended energy-loss fine structure (EXELFS), will also be averaged over all energies and will have a minimal effect on σ . (EXELFS is known to occur within about 100 eV of the ionization threshold).

III. RESULTS

A. K -shell ionization

Figure 2 shows the projected absorption potentials for K -shell ionization of constituent atoms in CdTe in Figs. 2(a) and 2(b), GaAs in Figs. 2(c) and 2(d), Si in Figs. 2(e) and 2(g), and diamond in Figs. 2(f) and 2(h), for 120 and 300 keV incident electrons. These graphs were obtained via the Fourier reconstruction Eq. (4), with at least 101 Fourier coefficients obtained by inserting each atom in a “cell” with an appropriate x dimension, and y and z dimensions chosen such that the atomic density was the same as that in the real crystal. The $\mathcal{A}[\text{kin}]$ term in Eq.

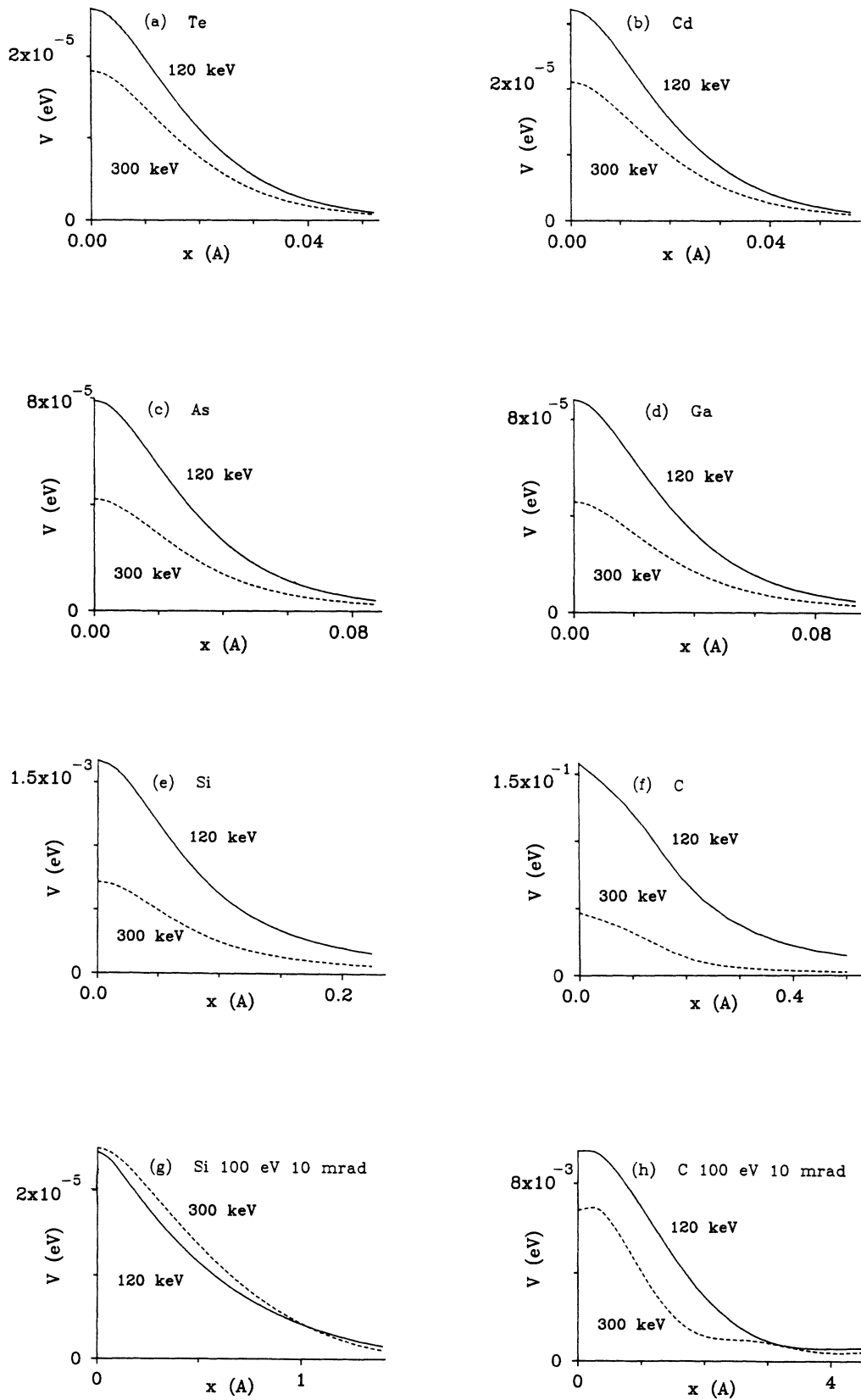


FIG. 2. Projected total K -shell ionization potentials $V''(r)$ for 120 and 300 keV electrons, for (a) Te, (b) Cd, (c) As, (d) Ga, (e) Si, and (f) C. Equivalent plots of $V''(r)$ for a limited energy window ΔE of 100 eV above threshold and semiangle $\Delta\theta$ of 10 mrad are shown for (g) Si and (h) C.

TABLE I. Incident beam energy E_0 , threshold energies E_T for K -shell ionization, and calculated full width at half maxima $V_{1/2}$ compared with rms impact parameters $\langle b^2 \rangle^{1/2}$.

Atom	E_0 (keV)	E_T (keV)	$V_{1/2}$ (Å)	$2\langle b^2 \rangle^{1/2}$ (Å)
Te	120	31.814	0.0354	0.0247
	300		0.0348	0.0186
Cd	120	26.711	0.0386	0.0255
	300		0.0382	0.0206
As	120	11.867	0.0593	0.0366
	300		0.0585	0.0351
Ga	120	10.367	0.0638	0.0396
	300		0.0632	0.0388
Si	120	1.839	0.1569	0.1346
	300		0.1504	0.1483
(EELS)				
10 mrad	120		0.9414	0.5206
100 eV	300		1.098	0.6390
diamond	120	0.284	0.3606	0.6193
	300		0.2934	0.7174
(EELS)				
10 mrad	120		3.094	2.570
100 eV	300		2.296	3.201

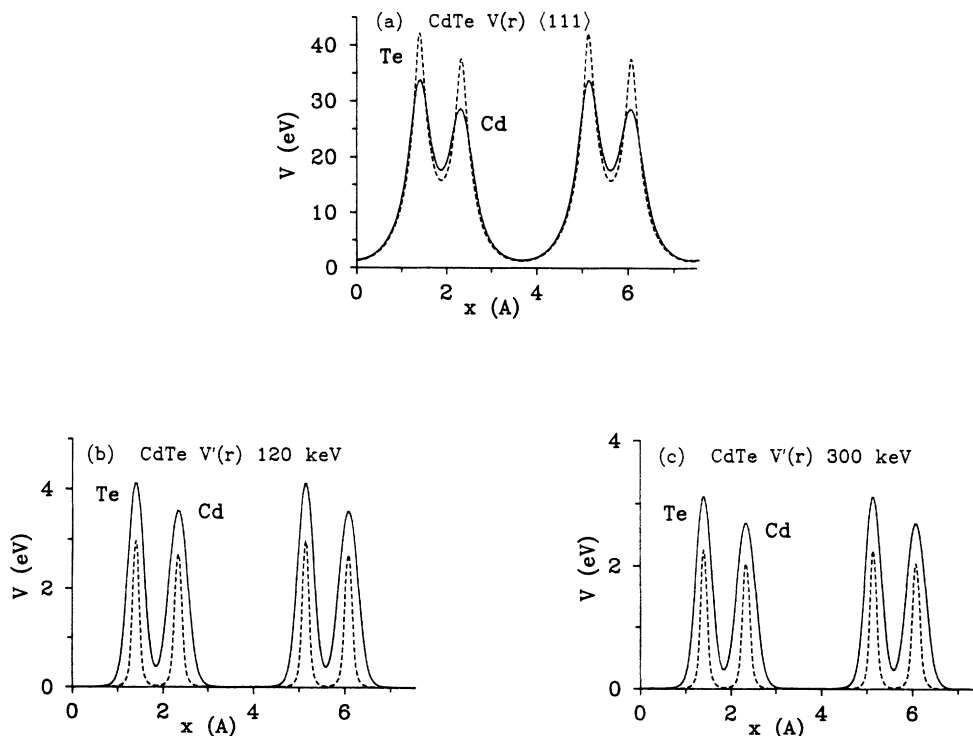


FIG. 3. CdTe potentials along the $\langle 111 \rangle$ projection for $T = 300$ K (solid line) and 0 K (dashed line) showing (a) elastic potential $V(r)$ and TDS potential $V'(r)$ for (b) 120 keV electrons and (c) 300 keV electrons.

(17) was obtained by integrating over a mesh of 20–50 equal steps in $\Delta\kappa$, and over a fine $\Delta\Omega$ mesh with $\Delta\theta = q_{\min}/5k$ (or about 1/5 of the characteristic angle θ_E), and $\Delta\varphi = \pi/6$ for nondiagonal terms. The length of the x axis on each graph is $1\frac{1}{2}$ times the full width at half maximum of the 120 keV potential, $V_{1/2}$. Note the increase in interaction delocalization with decreasing atomic number. For Si, $V_{1/2}$ is comparable to twice the rms thermal displacement at room temperature.

$V_{1/2}$ is related to the impact parameter $\langle b^2 \rangle$ pertinent to x-ray fluorescence,^{31–33} and is relatively insensitive to E_0 as shown in Table I. Here,

$$\langle b^2 \rangle^{1/2} = \frac{\hbar v}{\langle E \rangle} f, \quad (21)$$

where $\langle E \rangle$ is the mean energy loss associated with ionization [for integration over all final states $\langle E \rangle$ is typically 1.5–2 times the threshold ionization energy E_T (Ref. 28)] and f is a factor given by Bourdillon³² as roughly $\frac{1}{2}$, but more recently by Pennycook³³ for x rays (integration over all energies and all scattering angles) as

$$f = \left[\ln \left[\frac{E_0}{\langle E \rangle} \right] \ln \left[\frac{16E_0}{\langle E \rangle} \right] \right]^{-1/2} \quad (22)$$

so that $f \sim 0.68$ for Te K -shell ionization at 120 keV, and

$f \sim 0.13$ for C at 300 keV. For electron-energy-loss spectroscopy (EELS) (integration over limited energy window ΔE , so that $\langle E \rangle \sim E_T + \Delta E/2$), the formula for f is

$$f = \left[\ln \left[\frac{4E_0}{\langle E \rangle} \right] \right]^{-1/2}. \quad (23)$$

In Table I, $\langle E \rangle = 2E_T$ is assumed for x-ray fluorescence.

These results are similar to those of Glas and Henoc.³⁴ For x rays, higher incident energies lead to a slightly more localized interaction since a greater density of high- q channels are opened by integration over 4π steradians, leading to an increase in the mean momentum transfer. This integration over all final states yields an absorptive potential pertinent to x-ray fluorescence, where the final state of the scattered electron is not detected. Conversely, if the final state of the scattered electron is detected or apertured down to a defined maximum scattering angle θ_{\max} , higher-energy incident electrons can lead to a more delocalized interaction as observed by EELS, since smaller q channels exist for forward scattering. A plot of the absorptive potential for Si, integrating over an acceptance angle $\Delta\theta = 10$ mrad and $\Delta E = 100$ eV, is shown in Fig. 2(g). $V''(r)$ for 300 keV electrons is about 16% more delocalized than that for 120 keV electrons (see Table I), and about 6–7 times more

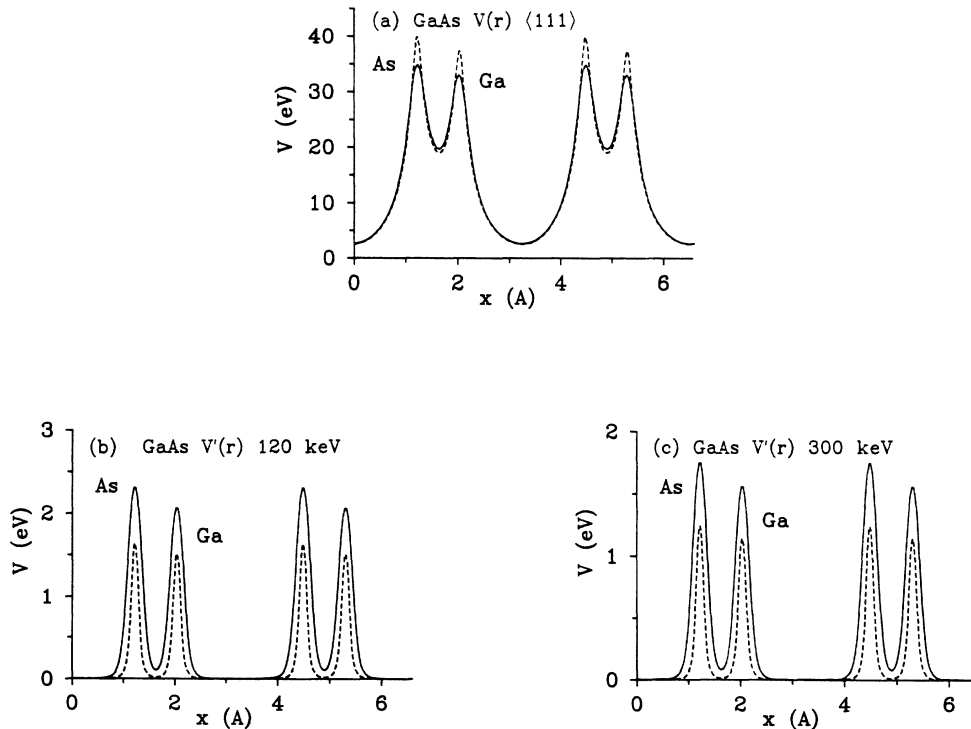


FIG. 4. GaAs potentials along the $\langle 111 \rangle$ projection for $T = 300$ K (solid line) and 0 K (dashed line) showing (a) elastic potential $V(r)$ and TDS potential $V''(r)$ for (b) 120 keV electrons and (c) 300 keV electrons.

delocalized than the potential for characteristic x-ray generation in Fig. 2(e). For carbon in Fig. 2(g), 300 keV electrons lead to a more localized potential than 120 keV electrons, and the delocalization in this case is about 8–9 times the value for x rays in Fig. 2(f).

B. Thermal diffuse scattering

Figures 3–6 show comparisons of the elastic potential $V(r)$ with $V'(r)$ for TDS as a function of temperature and incident beam energy, with kinematic mean free paths λ_{TDS} for the various crystals shown in Fig. 7. The graphs in Figs. 3–6 have an x axis projected along the $[111]$ crystal direction, the x dimension being $\frac{2}{3} [111]$ in length.

Data for CdTe and GaAs were derived from the thermal data of Reid,³⁵ i.e., $\Theta_{\text{Te}}=145$ K, $\Theta_{\text{cd}}=127$ K, $\Theta_{\text{GaAs}}=271$ K, and the well-known values $\Theta_{\text{Si}}=645$ K and $\Theta_{\text{dia}}=2230$ K for Si and diamond. The zero point fluctuation in atomic positions leads to a considerable absorptive potential, the lower Θ_D , the greater the relative change in λ_{TDS} and $V'(r)$ for 0 and 300 K. Note the change in λ_{TDS} by over an order of magnitude from diamond to CdTe [λ_{TDS} is inversely proportional to the area under the plots of $V'(r)$]. The leveling off of the curves at higher E_0 is a relativistic effect. Also shown for Si and diamond in Figs. 5(d) and 6(d) is a plot of $V''(r)$ for 120 keV electrons, for comparison with $V(r)$ and $V'(r)$. For Si, the ionization potential is more localized than the TDS potential, whereas for diamond $V''(r)$ has a distribu-

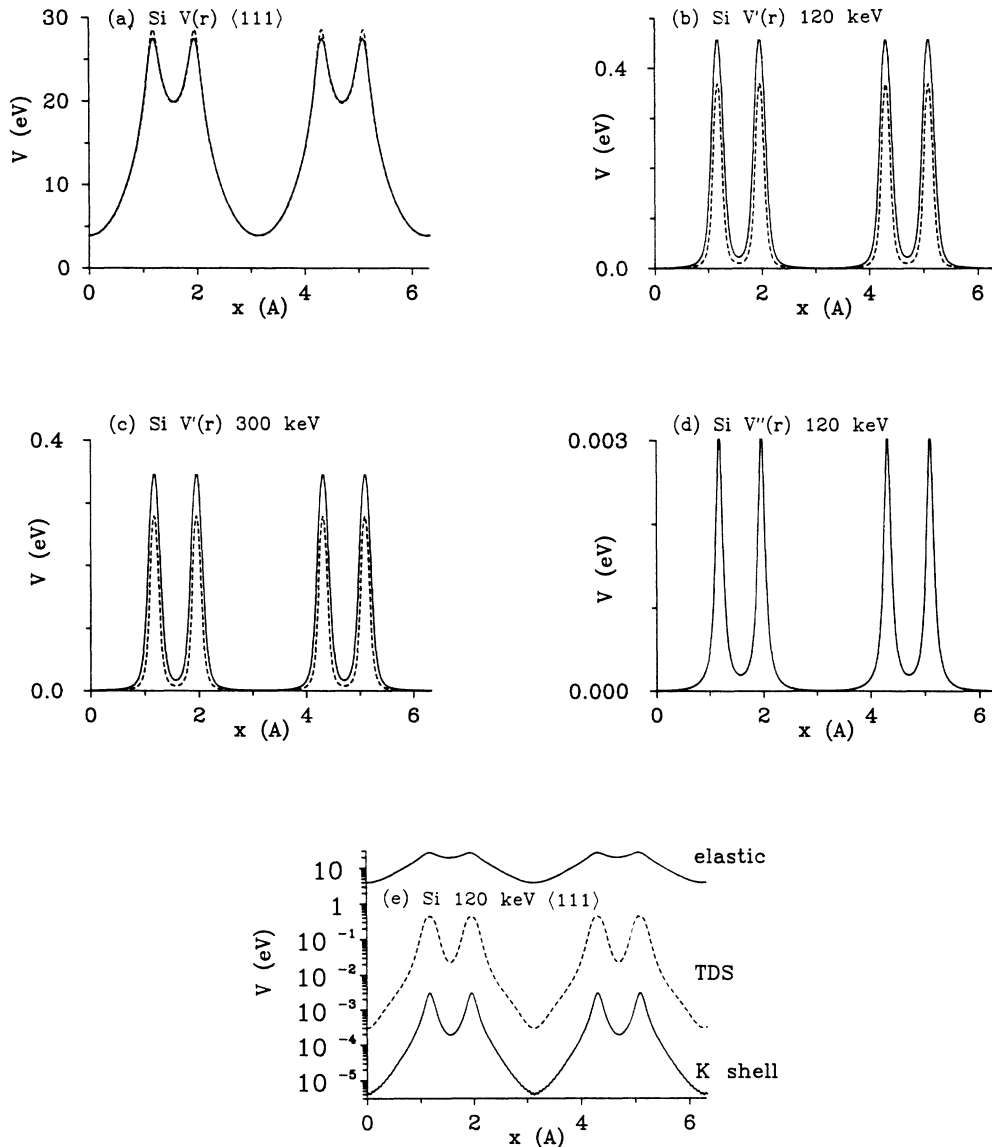


FIG. 5. Silicon potentials along the $\langle 111 \rangle$ projection for $T=300$ K (solid line) and 0 K (dashed line) showing (a) elastic potential $V(r)$ and TDS potential $V'(r)$ for (b) 120 keV electrons and (c) 300 keV electrons. $V''(r)$ for K -shell ionization is shown in (d), and all potentials at 300 K are compared in (e).

tion more characteristic of the elastic potential and is considerably more delocalized than the TDS potential. A comparison between the potentials $V(r)$, $V'(r)$, and $V''(r)$ for Si and diamond is shown on a logarithmic scale for 120 keV electrons in Figs. 5(e) and 6(e), revealing in more detail the behavior of $V''(r)$ between atomic positions.

The full width at half maximum of the TDS potential associated with each atomic site is roughly 4 times broader than the rms thermal displacement of individual atoms $\langle u^2 \rangle^{1/2}$, as shown in Table II.

The TDS absorptive potential is highly localized about atomic sites, and its small magnitude within empty crystal channels is in strong contrast with the elastic poten-

tial. The rapid truncation of the TDS potential away from the atomic sites leads to negative Fourier coefficients, as noted by Humphreys and Hirsch.¹² The Einstein model itself ensures that the Fourier coefficients are such that $V''(r)$ does not change sign in the open channels (were this to occur, spontaneous generation of fast electrons would be predicted for certain diffraction conditions). Note also the diminution of the TDS potential with increasing incident beam energy (the elastic potential is independent of incident beam energy), due to a smaller solid angle $d\Omega$ being available for a fixed momentum transfer q as the incident beam energy is increased.

Figure 8 shows computed ratios of $|V'_g|/|V_g|$ for CdTe

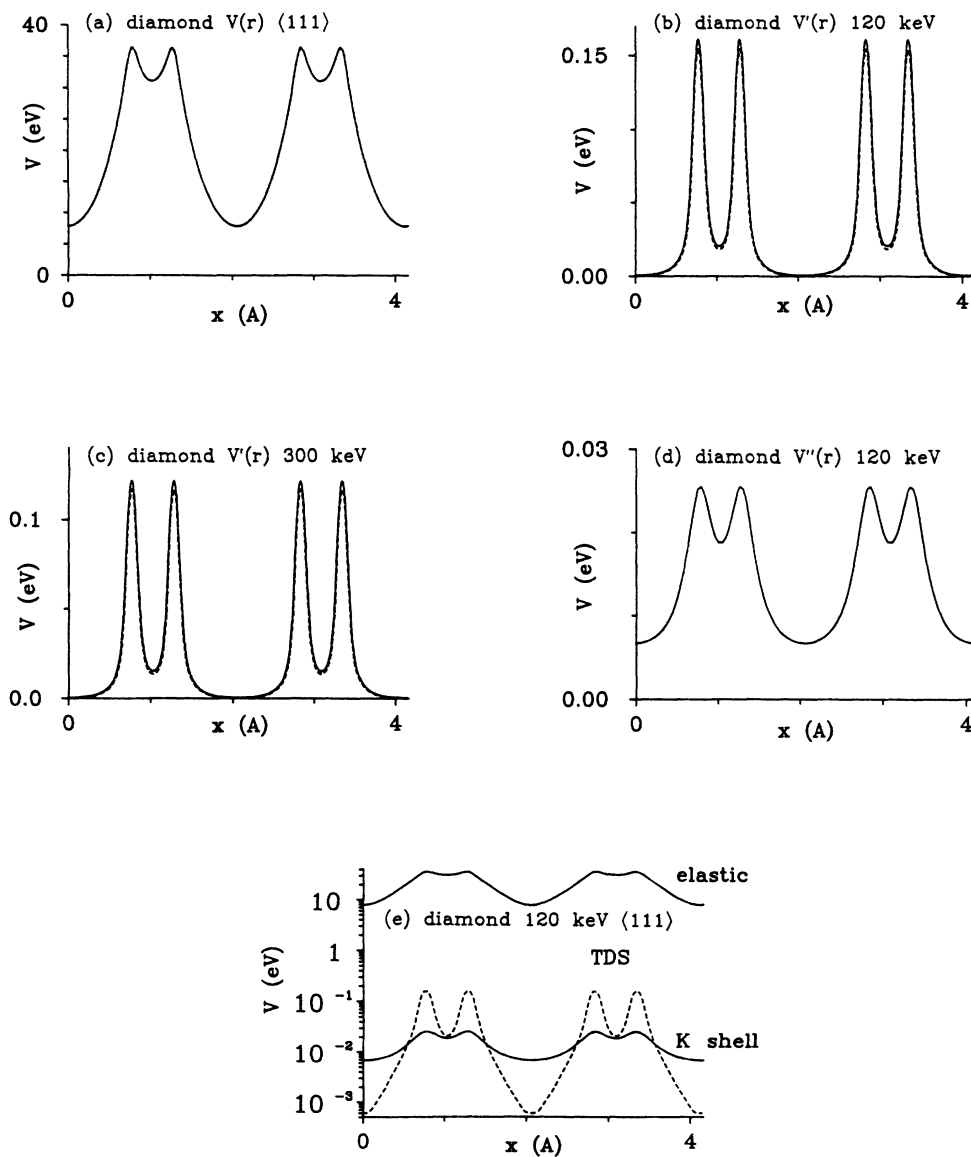


FIG. 6. Diamond potentials along the $\langle 111 \rangle$ projection for $T=300$ K (solid line) and 0 K (dashed line) showing (a) elastic potential $V(r)$ and TDS potential $V'(r)$ for (b) 120 keV electrons and (c) 300 keV electrons. $V''(r)$ for K-shell ionization is shown in (d), and all potentials at 300 K are compared in (e).

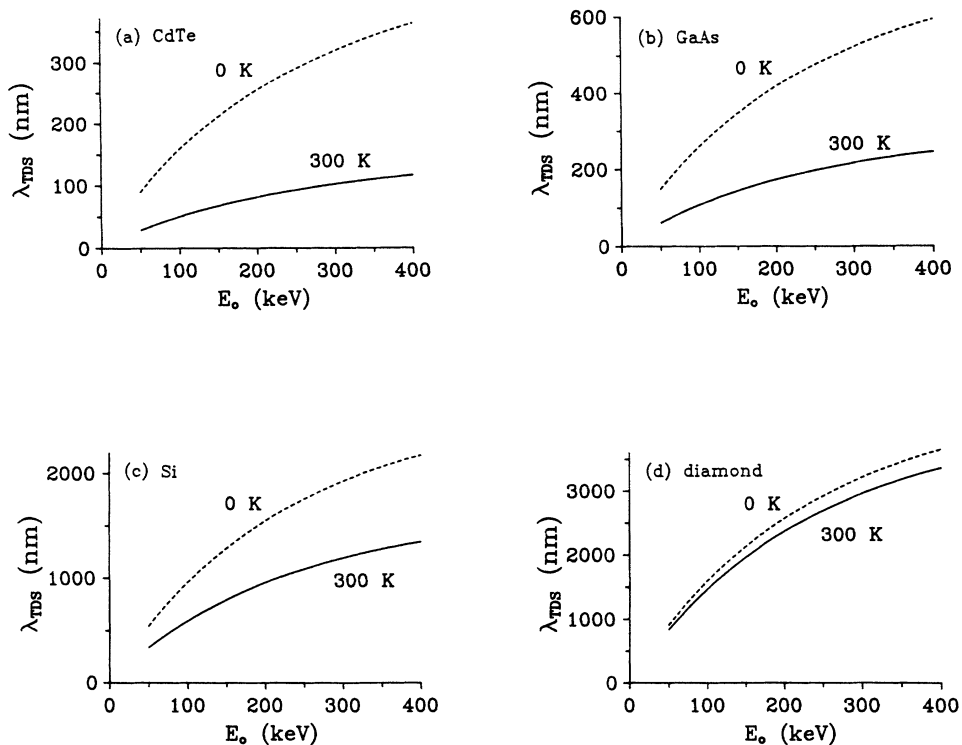


FIG. 7. Mean free paths λ_{TDS} for (a) CdTe, (b) GaAs, (c) Si, and (d) diamond for $T=0$ K (dashed line) and 300 K (solid line) as a function of incident beam energy.

for the (111) systematic row, and the change in phase angle $\Delta\varphi$ between the TDS absorptive values for V'_g and elastic values for V_g ($\Delta\varphi = \varphi' - \varphi$). Our results concur with those of Bird³⁸ for GaAs and other II-V semiconductors. If the approximation $V'(r) = \alpha V(r)$ is made, and α scaled such that λ_α under kinematic conditions is equal to λ_{TDS} from the Einstein model, this leads to smaller

anomalous but larger mean absorption components. Thus predicted "channeling" effects in sensitive diffraction experiments [such as large-angle convergent-beam electron diffraction (LACBED) patterns or high-resolution transmission electron microscope (HRTEM) images from relatively thick crystals] would be lower than that predicted from the Einstein model.

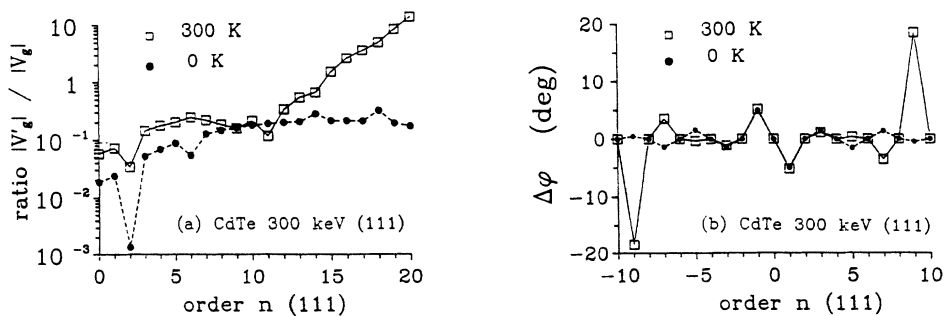


FIG. 8. (a) Ratios $|V'_g|/|V_g|$ for the systematic reciprocal-lattice row $g=n$ (111) for CdTe, 300 keV electrons and $T=0$ K (dashed line) and 300 K (solid line), as well as (b) the phase difference $\Delta\varphi = \varphi_{TDS} - \varphi_{elas}$ for the Fourier coefficients, as a function of n .

TABLE II. Full width at half maxima of TDS potentials associated with each atomic site, compared with rms thermal displacements of individual atoms for different temperatures.

Crystal	T (K)	$V_{1/2}$ (TDS) (Å)	$\langle u^2 \rangle^{1/2}$ (Å)
CdTe	0	Cd 0.193	0.050 65
		Te 0.172	0.044 48
	300	Cd 0.449	0.157 04
		Te 0.374	0.128 62
GaAs	0	Ga 0.180	0.044 01
		As 0.163	0.042 46
	300	Ga 0.353	0.090 56
		As 0.295	0.093 92
Si	0	0.188	0.044 95
	300	0.293	0.064 97
Diamond	0	0.172	0.036 98
	300	0.164	0.039 12

IV. DISCUSSION

The dynamical ionization cross section σ may be explicitly written in terms of Fourier components, coupled with eigenvalues and eigenvectors associated with the fast electron and excitation site as in Eq. (19). Values for σ_K (K -shell ionization) from the above formulation agree with the Egerton⁴ formulation for kinematic diffraction conditions and limited energy windows and scattering angles, and delocalization effects are generally consistent with impact parameter arguments. Our calculations suggest that the overall absorptive potential becomes slightly more localized with an increase in E_0 , as shown by the impact parameter formula of Pennycook.³³

The above method of calculating $V'(r)$ and $V''(r)$ due to TDS and K -shell ionization from first principles should enable a quantitative calculation of x-ray-emission yields

in crystals under strong dynamical diffraction conditions, accounting for both dechanneling effects (giving rise to a kinematical background) and interaction delocalization appropriately convoluted with thermal motion of atoms.^{34,36} This has many implications for analysis of impurity site distributions (ALCHEMI).^{21,37}

The above formulation also enables mean and anomalous absorption coefficients on different Bloch wave dispersion surfaces for TDS to be determined.^{21,38} Although low-energy plasmon losses may have a smaller mean free path λ_p than λ_{TDS} , electronic excitations are delocalized and tend merely to smear out diffraction contrast by inducing a small angular spread in the forward-scattered beam. The contribution from localized electronic excitations is relatively small. Thus TDS, by providing a mechanism for large momentum transfer with little energy loss or gain, is the predominant mechanism for altering diffraction contrast in HRTEM images or LACBED patterns by anomalous absorption. The theory presented in this paper has enabled quantitative correlation between calculated and experimental LACBED images³⁹ where anomalous absorption and changes in diffraction contrast are defined solely by the Debye-Waller factor for each crystal atom, there being no open parameters in the formalism. We are of the opinion that the common approximation, i.e., $V'(r) = \alpha V(r)$, cannot adequately describe anomalous absorption due to TDS. Our alternative approach, as initially proposed by Allen and Rossouw²¹ and subsequently by Bird and co-workers,^{22,38} enables quantitative calculation of TDS absorption from first principles. The absorptive potential is totally defined by $\langle u^2 \rangle$ and E_0 , and the use of the phenomenological factor α is avoided.

ACKNOWLEDGMENTS

We thank Dr. V. W. Maslen for helpful discussions. One of us (L.J.A.) acknowledges support for this work from the Australian Research Council.

- ¹V. W. Maslen and C. J. Rossouw, *Philos. Mag. A* **47**, 119 (1983).
- ²V. W. Maslen and C. J. Rossouw, *Philos. Mag. A* **49**, 735 (1984).
- ³C. J. Rossouw and V. W. Maslen, *Philos. Mag. A* **49**, 743 (1984).
- ⁴R. F. Egerton, *Ultramicrosc.* **4**, 169 (1979).
- ⁵M. J. Whelan, *J. Appl. Phys.* **36**, 2103 (1965).
- ⁶C. R. Hall and P. B. Hirsch, *Proc. R. Soc. London Ser. A* **286**, 158 (1965).
- ⁷C. J. Humphreys and P. B. Hirsch, *Philos. Mag.* **18**, 115 (1968).
- ⁸P. A. Doyle, *Acta Crystallogr. Sect. A* **26**, 133 (1970).
- ⁹G. Radi, *Acta Crystallogr. Sect. A* **26**, 41 (1970).
- ¹⁰C. J. Rossouw and L. A. Bursill, *Acta Crystallogr. Sect. A* **41**, 320 (1985).
- ¹¹C. J. Rossouw and L. A. Bursill, *Proc. R. Soc. London Ser. Sect. A* **408**, 149 (1986).
- ¹²C. J. Humphreys and P. B. Hirsch, *Philos. Mag.* **18**, 155 (1968).
- ¹³D. M. Bird, D. James, and Q. A. King, *Phys. Rev. Lett.* **63**,

1118 (1989).

¹⁴Z. L. Wang, *Acta Crystallogr. Sect. A* **45**, 636 (1989).

¹⁵P. Rez, C. J. Humphreys, and M. J. Whelan, *Philos. Mag.* **35**, 81 (1977).

¹⁶Z. L. Wang and J. M. Cowley, *Ultramicrosc.* **31**, 437 (1989).

¹⁷A. F. De Jong and K. T. F. Janssen, *European Conference on Electron Microscopy (1988) York, England, Inst. Phys. Conf. Ser. No. 93 (IOP, Bristol, 1988), Vol. 2, p. 153.*

¹⁸E. G. Bithell and W. M. Stobbs, *Philos. Mag. A* **60**, 39 (1989).

¹⁹A. F. De Jong and K. T. F. Janssen, *J. Mater. Res.* **15**, 578 (1990).

²⁰H. A. Bethe, *Ann. Phys. (Leipzig) [Folge 4]* **87**, 55 (1928).

²¹L. J. Allen and C. J. Rossouw, *Phys. Rev. B* **39**, 8313 (1989).

²²D. M. Bird and Q. A. King, *Proceedings of the 47th Annual Meeting of the Electron Microscopy Society of America*, edited by G. W. Bailey (San Francisco Press, San Francisco, 1989), p. 486.

²³D. M. Bird and Q. A. King, *Acta Crystallogr. Sect. A* **46**, 202 (1990).

²⁴P. A. Doyle and P. W. Turner, *Acta Crystallogr. Sect. A* **24**,

- 390 (1968).
- ²⁵D. T. Cromer and J. T. Waber, *Acta Crystallogr.* **18**, 104 (1965).
- ²⁶M. J. Whelan, *J. Appl. Phys.* **36**, 2099 (1965).
- ²⁷L. J. Allen, I. E. McCarthy, V. W. Maslen, and C. J. Rossouw, *Aust. J. Phys.* (to be published).
- ²⁸C. J. Rossouw and V. W. Maslen, *Ultramicrosc.* **21**, 277 (1987).
- ²⁹D. K. Saldin and P. Rez, *Philos. Mag. B* **55**, 481 (1987).
- ³⁰V. W. Maslen, *Philos. Mag. B* **55**, 491 (1987).
- ³¹A. J. Bourdillon, P. G. Self, and W. M. Stobbs, *Philos. Mag. A* **44**, 1335 (1981).
- ³²A. J. Bourdillon, *Philos. Mag. A* **50**, 839 (1984).
- ³³S. J. Pennycook, *Ultramicrosc.* **26**, 239 (1988).
- ³⁴F. Glas and P. Henoc, *Philos. Mag. A* **56**, 311 (1987).
- ³⁵J. S. Reid, *Acta Crystallogr. A* **39**, 1 (1983).
- ³⁶D. Cherns, A. Howie, and M. H. Jacobs, *Z. Naturforsch.* **28a**, 565 (1973).
- ³⁷P. S. Turner, T. J. White, A. J. O'Connor, and C. J. Rossouw, *J. Microsc.* (to be published).
- ³⁸D. M. Bird, *Acta Crystallogr. Sect. A* **46**, 208 (1990).
- ³⁹C. J. Rossouw, P. R. Miller, L. J. Allen, and J. Drennan, *Ultramicrosc.* (to be published).

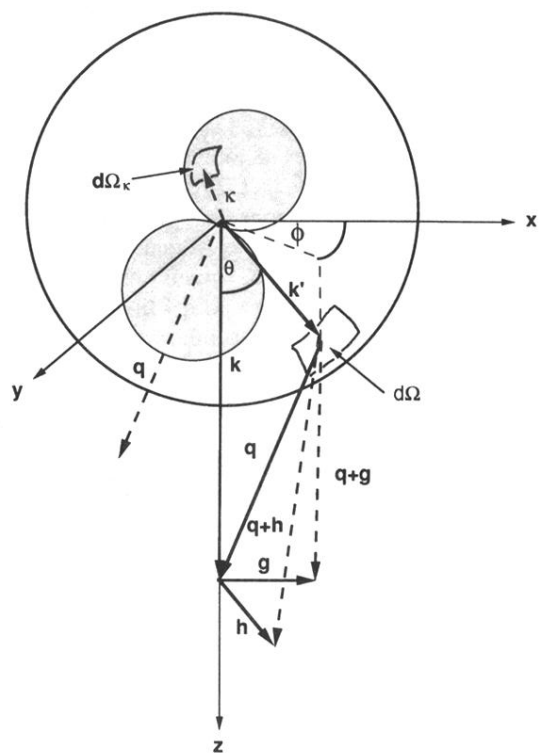


FIG. 1. Reciprocal space diagram showing relationships between quantities relevant to K -shell ionization (see text for details). The shaded area indicates a p -type lobe for the ejection probability of an inner K -shell electron for a small “diagonal” q term.